Nanoscale

COMMUNICATION

View Article Online
View Journal

Cite this: DOI: 10.1039/d5nr03987h

Received 21st September 2025,
Accepted 7th March 2026

DOI: 10.1039/d5nr03987h

rsc.li/nanoscale

Phonon modulation of strongly coupled gold tetrahedral plasmonic nanoparticles and a carbocyanine J-aggregate

Bailey M. Chandler,[a] Fanrui Cheng,[b] Yi Wang,[b] Xingchen Ye,[b] George C. Schatz,[a] Lin X. Chen *[a,c] and Richard D. Schaller *[a,d,e]

Coupling exciton and plasmon excitations to form polaritons are of great interest for manipulating energy transfer at the nanoscale *via* the formation of hybrid light–matter states. In this study, we successfully couple gold tetrahedral nanoparticles with the J-aggregate forming dye 5,5′,6,6′-tetrachloro-1,1′-diethyl-3,3′-di(4-sulfobutyl)-benzimidazolocarbocyanine (TDBC) to form a strongly coupled colloidal polariton system with a Rabi splitting energy of ~206 meV. These gold tetrahedra exhibit coherent phonon modes upon photoexcitation, which produce transient oscillations of the LSPR energy for isolated tetrahedra. Transient absorption measurements of the polariton system were performed and show how these coherent phonon modes influence the polariton states' extinction. We found that the oscillation period increases by 0.5 ± 0.14 ps upon surface deposition of TDBC dye, demonstrating LSPR sensitivity to the refractive index environment. Shifts in the plasmon resonance due to the coherent phonon modes transiently alters LSPR alignment with the J-aggregate exciton peak, resulting in shifts of the hybrid polariton states' oscillator strength.

Introduction

Manipulation of light–matter interactions at the nanoscale is of great interest for several prospective nanophotonic devices and applications. Polaritons refer to coupled excitations resulting from plasmonic–excitonic hybridization and exhibit energy states and lifetimes that differ from either the plasmon or exciton alone.[1–3] Nanoparticles that support a localized surface plasmon resonance (LSPR) can confine light to sub-wavelength scales, achieving rather small electromagnetic field mode volumes.[1,4–6] By placing an excitonic material with optical transitions near resonance with the LSPR proximally to this plasmonic cavity, coupling can occur.[1,4] When weakly coupled, the plasmonic cavity may enhance the molecule's spontaneous emission rates *via* a process known as the Purcell effect.[2,4–8] Strong coupling, however, causes the formation of new hybrid light–matter states termed polaritons. To achieve strong coupling, the plasmon and exciton must coherently exchange energy at a rate faster than either dissipation of light from the plasmonic cavity or decay of the exciton.[1,2,4,5,9,10] Colloidal polaritons can be formed through low cost, scalable, wet chemical synthesis and assembly, making them a desirable route for controlling light interactions and the energy flow at the nanoscale.[11–13] J-aggregate molecular dyes are often selected for coupling, as their excitonic transitions have high oscillator strengths and narrow linewidths, indicative of exciton delocalization that fosters stronger coupling to the plasmon.[5,14,15] Furthermore, synthetically they can be coupled to nanoparticles through manipulation of electrostatic interactions between the nanoparticle capping layer and the dye molecule.[16–18] The hybrid upper and lower polariton states formed are separated by a characteristic Rabi splitting energy (Ω), with a transparency dip, commonly referred to as the avoided crossing region, separating the two states.[2,4,5]

The strength of coupling can be described by the Tavis–Cummings Hamiltonian. This model describes N number of identical two-level molecules coupled to a cavity with breadth in frequency.[1,4,19] From this model, the coupling strength is derived to be proportional to $\frac{\sqrt{N}}{\sqrt{V}}$ where N is the number of molecules coupled to the plasmonic cavity and V is the mode volume of light confined within the cavity.[1,4] In addition to the small mode volume of the plasmonic nanoparticle increasing the coupling strength, it is also advantageous to couple a high number of molecules to the cavity.[20] The strong coupling regime is reached when the coupling strength is greater than

[a]Department of Chemistry, Northwestern University, Evanston, Illinois, 60208, USA. E-mail: l-chen@northwestern.edu, schaller@anl.gov
[b]Department of Chemistry, Indiana University, Bloomington, Indiana, 47405, USA
[c]Chemical Sciences and Engineering Division, Argonne National Laboratory, Lemont, Illinois 60439, USA
[d]Center for Nanoscale Materials, Argonne National Laboratory, Lemont, Illinois 60439, USA
[e]International Institute for Nanotechnology; Paula Trienens Institute for Sustainability and Energy, Northwestern University, Evanston, IL 60208, USA

the rates of dissipation of both the plasmonic cavity and the exciton dipole. Such a requirement can be described in the inequality $2\Omega > \kappa + \gamma$, where Ω is the Rabi splitting energy, κ is the dissipation rate of the cavity, and γ is the dissipation rate of the dipole excitation.[2,4]

Beyond static measurements to determine the coupling strength, ultrafast transient studies can reveal the lifetimes of these hybrid polariton states.[20–25] Additionally, plasmonic nanoparticles exhibit coherent phonon breathing modes upon photoexcitation, causing expansions and contractions of the nanoparticle lattice.[26] The plasmon energy is highly sensitive to deformations of the lattice, and thus oscillations of the LSPR are observable in transient absorption studies. These acoustic phonon modes can modulate polariton coupling, as demonstrated in gold bipyramidal samples coupled with the thiacarbocyanine dye, 2,2′-dimethyl-8-phenyl-5,6,5′,6′-dibenzothiacarbocyanine chloride (TCC) dye.[27] Phase manipulation of these phonon modes in polariton systems has also been demonstrated for optical switching and memory applications.[28]

Gold nanotetrahedra are promising candidates for polariton formation, as they can be synthesized in highly monodisperse batches and have sharp corners and edges which offer strong EM field confinement.[29,30] The synthetic control over corner sharpness offers an additional avenue for potential modulation of coupling strength. In this study, a colloidal polariton system of gold nanotetrahedra strongly coupled to the J-aggregate forming dye TDBC (5,5′,6,6′-tetrachloro-1,1′-diethyl-3,3′-di(4-sulfobutyl) benzimidazolocarbocyanine) was synthesized. Static and transient optical measurements were carried out to measure the Rabi splitting energy and phonon mediation of the polaritons. When the LSPR energy was near resonant with the J-aggregate peak of TDBC, a maximal splitting energy of 244 meV was observed. By fitting the upper and lower polariton resonances to a coupled harmonic oscillator, the characteristic Rabi splitting energy was found to be 206 meV, which is greater than or comparable to other plasmonic systems coupled with the J-aggregate of TDBC. Transient absorption studies revealed that the extinction of the polariton states' bleach feature is modulated by the expansion and contraction of the nanoparticle lattice, as the plasmon resonance feature periodically oscillates between higher and lower energies, shifting its overlap with the exciton feature. The phonon modes of the bare nanotetrahedra were previously characterized, and the nanoparticles were shown to exhibit a primary breathing mode that causes the corners of the tetrahedra to expand outward.[31] Transient absorption measurements were performed off resonance, obscuring any modulation to the Rabi splitting energy, but still allowing for observations to changes in the polariton extinction as a function of phonon mode. Additionally, the phonon mode periods are shown to increase by ~0.5 ps across all samples upon addition of mass from the dye. Future studies altering the amount of dye added to the nanoparticle ensemble may further determine the phonon mode's sensitivity to additional mass.

Results and discussion

A size series of highly monodisperse gold nanotetrahedra, referred to herein by their peak LSPR wavelength, were coupled with TDBC dye. These nanoparticles were carefully selected to have an LSPR energy resonant or nearly resonant with the J-aggregate exciton transition in TDBC. The plasmonic nanoparticles are highly monodisperse as shown in the TEM images in Fig. S1, which helps to decrease dissipation rates of the plasmon and enhance the coupling strength. The nanoparticle samples were capped by positively charged CTAC, while TDBC dye molecules carry a negative charge; thus, associations between the two systems occurred *via* electrostatic coupling and van der Waals interactions.

Fig. 1A shows the extinction spectra for TDBC, gold tetrahedral nanoparticles, and coupled TDBC–gold nanoparticles, all dispersed in water. TDBC assembles into J-aggregates in water, resulting in a strong, narrow excitonic absorption peak centered at 587 nm. Each hybrid sample exhibits split peaks, with a transparency dip occurring near the TDBC J-aggregate absorption peak. For samples with greater detuning energy between the plasmon and exciton, the hybrid peaks form an antisymmetric Fano resonance line shape, as expected from polariton formation.[5,27] Titrations, presented in Fig. 1B, were performed to discern the effect of dye concentration on Rabi splitting energy for the gold tetrahedra with the LSPR at 595 nm, which is nearly resonant with the exciton energy. When twice as much dye was added to the sample, the Rabi splitting energy increased by a factor of approximately $\sqrt{2}$, as predicted by the Tavis–Cummings model. Adding greater quantities of dye beyond this point did not significantly increase the splitting energy. This dependence on dye concentration would suggest that a strong coupling regime has been reached. The change in peak splitting as a function of detuning energy is presented in Fig. 1C. A clear avoided crossing region between the upper and lower polariton features is distinct, with the greatest Rabi splitting energy occurring in the samples with near resonant overlap between the plasmon and exciton. To accurately determine the Rabi splitting energy for the system, the upper and lower polariton resonances were fit to a coupled harmonic oscillator model as follows:

$$E(\hbar\omega_p) = \frac{\hbar\omega_p + \hbar\omega_0}{2} \pm 0.5\sqrt{(\hbar\Omega_r)^2 + (\hbar\omega_p - \hbar\omega_0)^2} \quad (1)$$

where $\hbar\omega_p$ is the LSPR energy, $\hbar\omega_0$ is the exciton energy, and $\hbar\Omega_r$ is the Rabi splitting energy.[27]

To further ascertain if strong coupling was reached, the Rabi splitting energies for each sample were compared with the dephasing rates of the plasmon and exciton. The dissipation rates for the gold tetrahedral nanoparticles and TDBC were estimated by fitting the LSPR and excitonic peak to a Lorentzian and Gaussian, respectively, to determine the full width at half maximum (FWHM).[4] Likewise, the wavelengths for the upper and lower polariton peak maximums were estimated *via* Lorentzian fits. The splitting energy was then calculated by taking the difference in the energy of the peak posi-

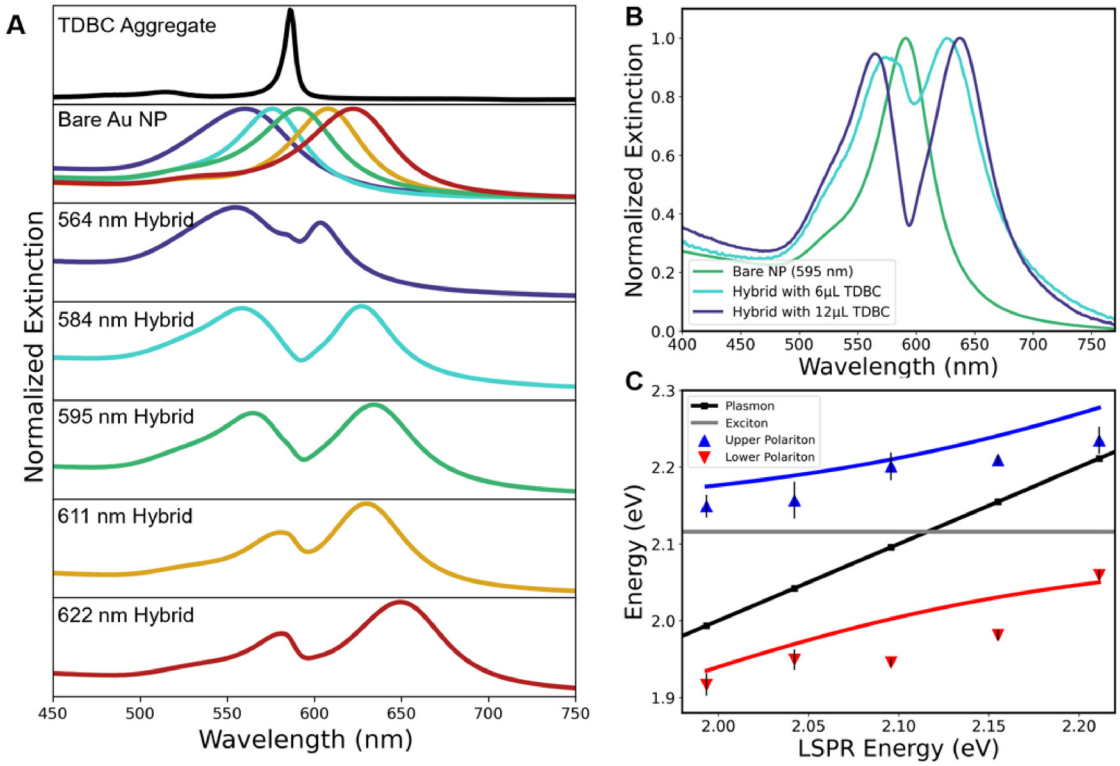

Fig. 1 (A) Static extinction for TDBC aggregate, gold tetrahedral nanoparticles, and polariton systems dispersed in water. LSPR of gold tetrahedron samples ranges from 564–622 nm. (B) Static extinction spectra for the 595 nm sample titrated with varying amounts of TDBC. (C) Upper and lower polariton energies as a function of LSPR energy.

Table 1 Dissipation rates (k and γ) of the LSPR and exciton, peak positions of the upper polariton (UP) and lower polariton (LP), and Rabi splitting energies Ω

LSPR (nm)	k_{LSPR} (eV)	γ_{TDBC} (eV)	UP (eV)	LP (eV)	Ω (eV)	$\frac{2\Omega}{\gamma_{\mathrm{TDBC}}+k_{\mathrm{LSPR}}}$
564	$0.302 \pm 2 \times 10^{-3}$	$0.03 \pm 1 \times 10^{-3}$	2.23 ± 0.02	2.06 ± 0.01	0.18 ± 0.02	1.18
584	$0.171 \pm 2 \times 10^{-3}$	$0.03 \pm 1 \times 10^{-3}$	2.21 ± 0.01	1.98 ± 0.01	0.23 ± 0.01	2.64
595	$0.180 \pm 2 \times 10^{-3}$	$0.03 \pm 1 \times 10^{-3}$	2.20 ± 0.01	1.95 ± 0.01	0.26 ± 0.02	2.84
611	$0.170 \pm 2 \times 10^{-3}$	$0.03 \pm 1 \times 10^{-3}$	2.16 ± 0.02	1.95 ± 0.01	0.21 ± 0.03	2.43
622	$0.183 \pm 2 \times 10^{-3}$	$0.03 \pm 1 \times 10^{-3}$	2.15 ± 0.01	1.92 ± 0.01	0.23 ± 0.02	2.47

Error for UP, LP, and Ω determined by measuring samples in triplicate.

tion of the lower and upper polaritons. These results are presented in Table 1.

The gold tetrahedron sample with LSPR at 584 nm reached a maximum Rabi splitting energy of ~244 meV. It may be noted that slight alterations to nanoparticle size to provide greater overlap may increase this splitting energy. The inequality for determining the strong coupling regime was rearranged as follows:

$$\frac{2\Omega}{\kappa+\gamma} > 1.$$

For each sample, this inequality yielded a value larger than 1, indicating that the coherent exchange of energy in the polariton hybrids occurs faster than dissipation of the plasmon or exciton, further supporting the hypothesis that strong coupling has been achieved. The high Rabi splitting energy of 206 meV modeled by coupled harmonic oscillators may be due in part to the sharpness of the corners of the tetrahedra, which increases the electric field focusing at the tips. Whether the J-aggregate coupling is the strongest for the face, edges, or corners of the tetrahedra likely impacts the coupling strength and could be a matter of future study. We find that this splitting energy is greater than or comparable to similar plasmonic–excitonic nanoparticle systems encapsulated with CTAC/CTAB ligands and coupled with TDBC dye, such as gold nanostars (145 meV), gold trigonal bipyramids (155 meV), and gold nanocubes (215 meV).[32]

Ultrafast transient absorption studies were then performed to analyze the role of impulsively excited nanoparticle phonon

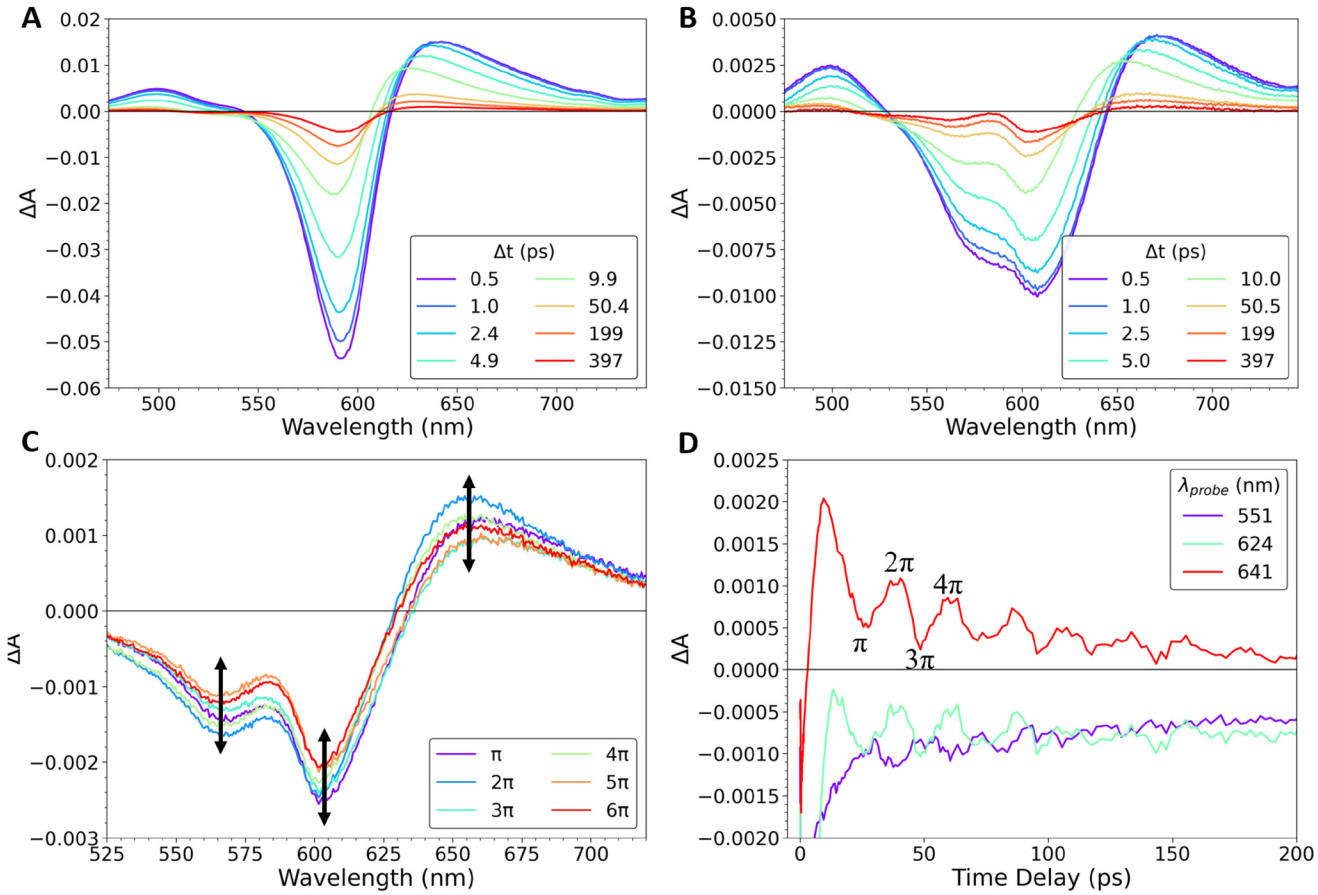

Fig. 2 (A) Transient absorption spectra for 595 nm bare nanoparticles and (B) polaritonic nanoparticles. (C) The spectral shapes for the polariton are additionally presented as a function of the phonon phase, corresponding to the maximum contraction or expansion of the lattice. Black arrows indicate the oscillations in extinction coefficient at the bleach and absorption features. (D) Kinetic traces showing oscillations caused by nanoparticle phonon modes.

modes in polariton coupling. Transient absorption spectra for the bare nanoparticles with LSPR at 595 nm and their polariton hybrids are shown in Fig. 2. As these samples were excited off resonance at 450 nm, the early times are dictated by plasmonic dynamics, namely electron–electron and electron–phonon scattering. Two ground state bleach features emerge in the hybrid system, corresponding to the upper polariton state and the slightly red-shifted plasmon resonance. Observation of the uncoupled plasmon feature in the hybrid system may be due to the off-resonance excitation conditions, as reported in other previous studies.[22] Due to spectral congestion of transient signals arising from shifting of both polariton features and background components, analysis of Rabi coupling strength modulation is challenging. However, we do clearly observe the oscillatory behavior of the upper polariton extinction coefficient, especially at the position of the bleach feature, as modulated by the phonon motion.

Photoexcitation of the nanoparticles launches coherent acoustic phonon modes, resulting in oscillatory features across the spectral probe region. Expansion of the nanoparticle lattice due to the primary phonon breathing mode corresponds with an observable redshift of the LSPR, while contraction corresponds to a blueshift.[31] To better understand these features and their impact on polaritonic features, time-resolved spectra were plotted as a function of the phonon phases, π, which are observable in the transient kinetic traces and represent the points of maximum and minimum expansion. The odd π phases indicate expansion of the nanoparticle lattice where the LSPR red shifts, while even π phases indicate contraction of the lattice where the LSPR blue shifts. Red shifting of the LSPR reduces resonance overlap with the exciton feature at 587 nm. As a result, the odd π phases in the transient spectra demonstrate a decrease in the absolute value of ΔA for the upper polariton bleach feature. The inverse is observed as the lattice contracts and greater overlap with the LSPR and exciton occurs. Furthermore, a small shift in the upper polariton bleach is observed over time, evolving from 567 nm to 562 nm, respectively, with expansion and contraction. While the obscurement of the lower polariton by the plasmon makes it difficult to discern whether the Rabi splitting energy changes transiently, these features do suggest a modulation of the upper polariton's extinction coefficient as a function of the phonon modes.

Similar effects can be observed for nanoparticle systems with greater detuning between the LSPR and exciton. The 564 nm and 622 nm samples have LSPR energies higher and lower than the TDBC's J-aggregate exciton resonance, respectively. As a result, while contraction of the nanoparticle lattice will increase the overlap of the plasmon and exciton feature in the red-detuned 622 nm sample, it will decrease overlap for the blue-detuned 564 nm sample. The inverse is true for expansion of the lattice. As a result, the polariton bleach feature in each sample reaches a more negative extinction coefficient at different phases of the phonon mode, as shown in Fig. 3. For the blue-detuned 564 nm sample, the maximally negative extinction coefficients occur at the odd-numbered pi phases when the lattice expands, while the red-detuned 622 nm samples show maximum extinction coefficients at the even-numbered π phases, when the lattice contracts.

As these spectral signatures are complex, to further deconvolute the role the phonon mode in modulating polariton signals, oscillation associated spectra (OAS) were generated. Using a previously established matrix pencil method, each wavelength was fit to a sum of complex exponentials and the non-oscillatory components were subtracted.[28] From here, a Fourier transform at every probe wavelength was performed and averaged. The oscillatory phases for plasmonic nanoparticles observed in transient absorption are straightforward, either being perfectly in phase or out of phase by 180 degrees. Due to this simplicity, the relative phase behavior of a given oscillation can be assigned a value of 1 when in phase with initial lattice expansion and −1 when out of phase.[28] From here, a contour map of the relative oscillation phase multiplied by the Fourier transform magnitude can be generated, labeled the OAS. The Fourier transforms as a function of oscillatory period and the 2D OAS for the 595 nm bare tetrahedra and polariton samples are shown in Fig. 4.

The Fourier transform shows a very small shift in period from 22.89 for the bare nanoparticle to 23.38 ps for the polariton hybrid, likely as a result of the increase in mass and the changes to the immediate refractive index environment. The Fourier transforms of the remaining samples were also performed, and the average change in period was determined to be 0.5 ± 0.14 ps. In the 2D OAS map, the dark blue *versus* yellow contours represent oscillatory features which are 180 degrees out of phase with each other. Plasmonic nanoparticle acoustic phonon modes have previously been demonstrated to exhibit oscillations of opposite phases on either side of the LSPR. For the bare nanoparticles shown in the 2D OAS map, this flip is observable near 595 nm, the position of the LSPR, and the oscillations here range in wavelength from ~550 to 650 nm. By comparison, the polariton nanoparticles present oscillations ranging from 520 nm to as red as 690 nm, demonstrating that polariton features with energies higher or lower than the plasmonic bleach still experience the effects of coherent oscillations. Additionally, the phase flip appears centered at 605 nm, the position of the plasmonic bleach observed in TA. The polariton case shows a larger separation in wavelength between the two phases in contrast to the bare nanoparticles. In addition to illustrating the nanoparticle LSPR sensitivity to mass, this demonstrates that the position of the upper polariton overlaps with one phase of the nanoparticle's phonon mode and thus will oscillate in position. To further illustrate the influence of coherent phonons on the LSPR peak position and overlap with the exciton feature, a slice of the OAS taken at the frequency of the maximum FT magnitude has been plotted against the static extinction spectra for the bare nanoparticle (Fig. 5A) and polariton hybrid (Fig. 5B).

The coherent phonon modes of bare plasmonic nanoparticles cause the LSPR to oscillate in peak position, changing the LSPR's maximum extinction wavelength while only slightly broadening the peak.[28] The extinction at a given wavelength is thus dependent on its proximity to the new LSPR peak position. Taking the first derivative of the static extinction spectrum with respect to energy can illustrate this phenomenon, assuming the peak does not significantly broaden, and should align with the OAS slice.[28] For the bare

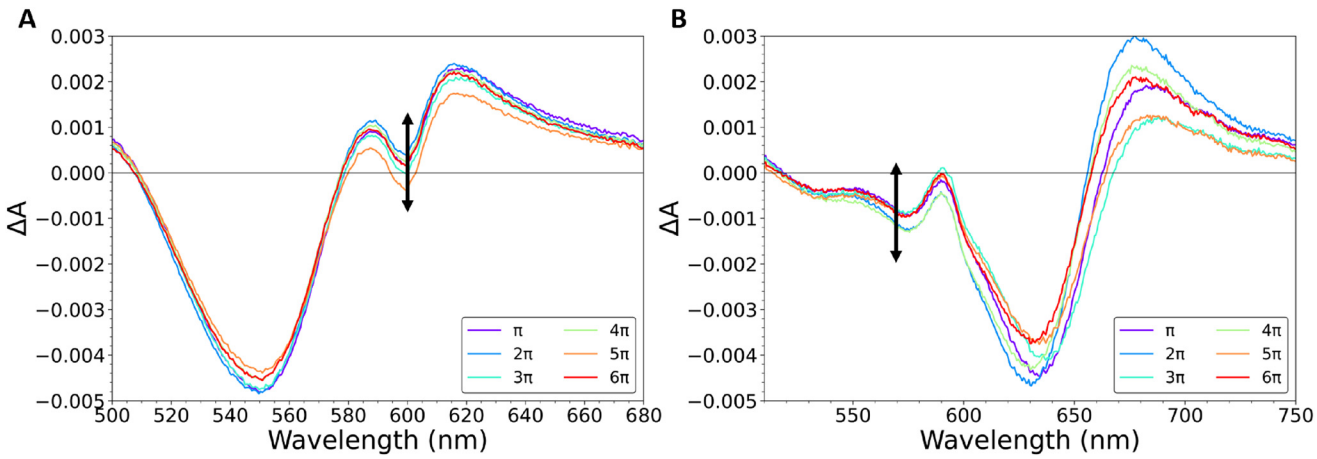

Fig. 3 Transient absorption spectra for samples with higher (A) and lower (B) LSPR energy. For the sample with LSPR at 564 nm, the lower polariton is visible, while for the sample at 622 nm, the upper polariton is visible. Black arrows show oscillations of the polariton bleach feature.

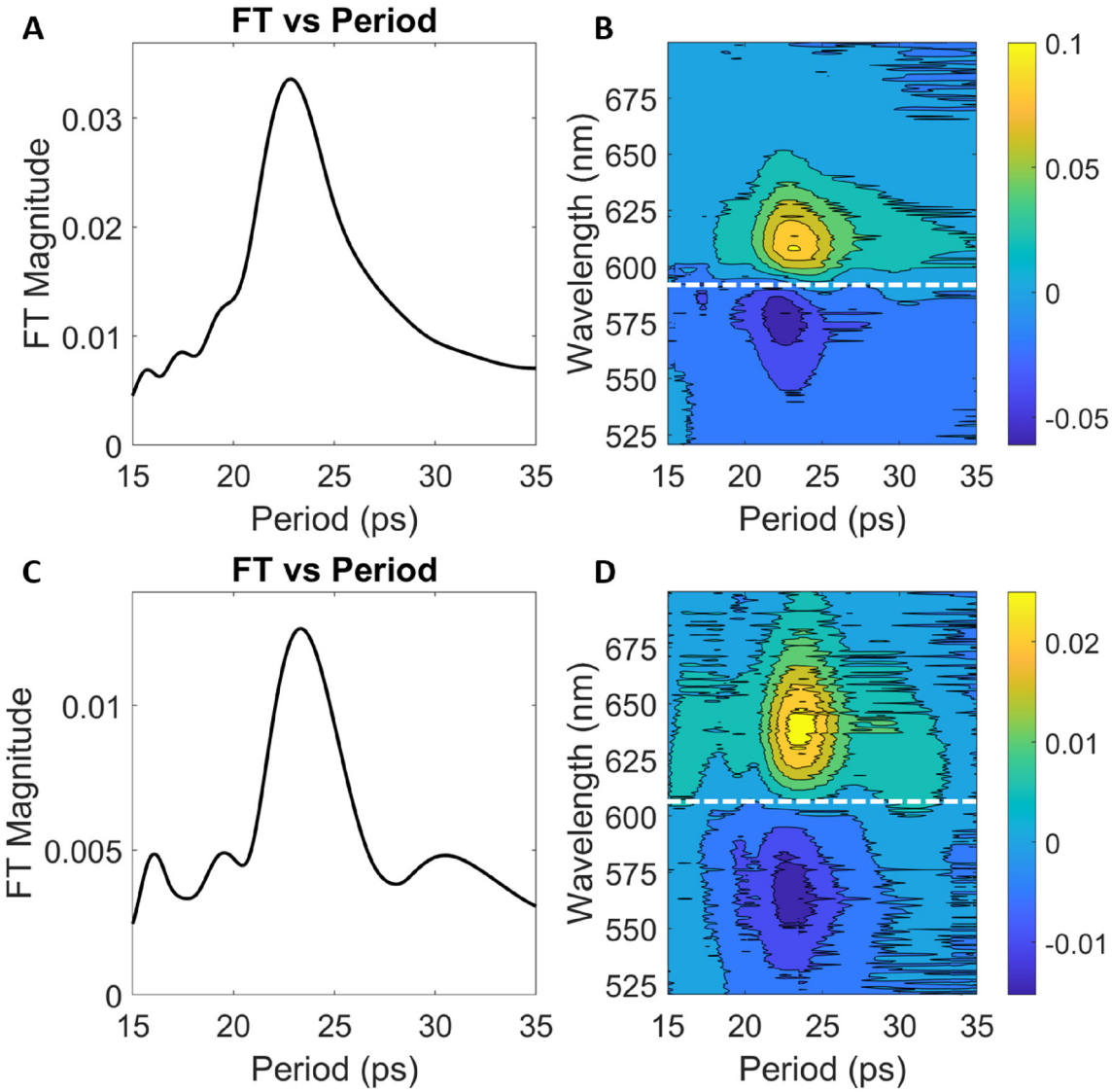

Fig. 4 Averaged Fourier transform as a function of the period of oscillation for (A) LSPR = 595 nm bare nanoparticles and (C) polariton hybrids. 2D oscillation associated spectra for (B) LSPR = 595 nm bare nanoparticles and (D) polariton nanoparticles. Dashed white line highlights the wavelength where oscillations flip 180 degrees in phase.

nanoparticle, the first derivative and OAS taken at a period of 23.38 ps do align very well. Subtracting the OAS from the static extinction spectrum further shows that the LSPR only red and blue shifts as expected, shown in the inset of Fig. 5A, illustrating how the coherent phonons can modulate the alignment of the LSPR and the exciton peak once the dye has been coupled to the system. The OAS slice (taken at a period of 23.38 ps) for the polariton hybrid was then examined. Notably, the first derivative with respect to the energy of the polariton static spectrum does not fully align with the OAS, likely due to the dominance of the plasmonic bleach feature in the transient spectra. This suggests that the oscillatory features observed are solely arising from the plasmonic feature, rather than the polariton hybrids. Thus, while the magnitude of ΔA for the polariton bleach in the transient data oscillates in response to the phonon mode, it is unlikely that the Rabi coupling strength between the two polariton features is being modulated.

A semi-phenomenological theory that describes the transient absorption results in this paper can be developed by combining the coupled oscillator model in eqn (1) with oscillations in the plasmon frequency ω_p due to acoustic mode excitation, then adding this result to a formula for the extinction lineshape function, and then including the effect of bleaching and excited state absorption on the transient absorption signal. If the Rabi frequency does not vary with acoustic excitation and the plasmon frequency is a simple periodic function of time, then eqn (1) is modified to:

$$E(\hbar\omega_{\mathrm{pol}\pm}(t)) = \frac{\hbar\omega_p(t) + \hbar\omega_0}{2} \pm 0.5\sqrt{(\hbar\Omega_r)^2 + (\hbar\omega_p(t) - \hbar\omega_0)^2} \quad (2)$$

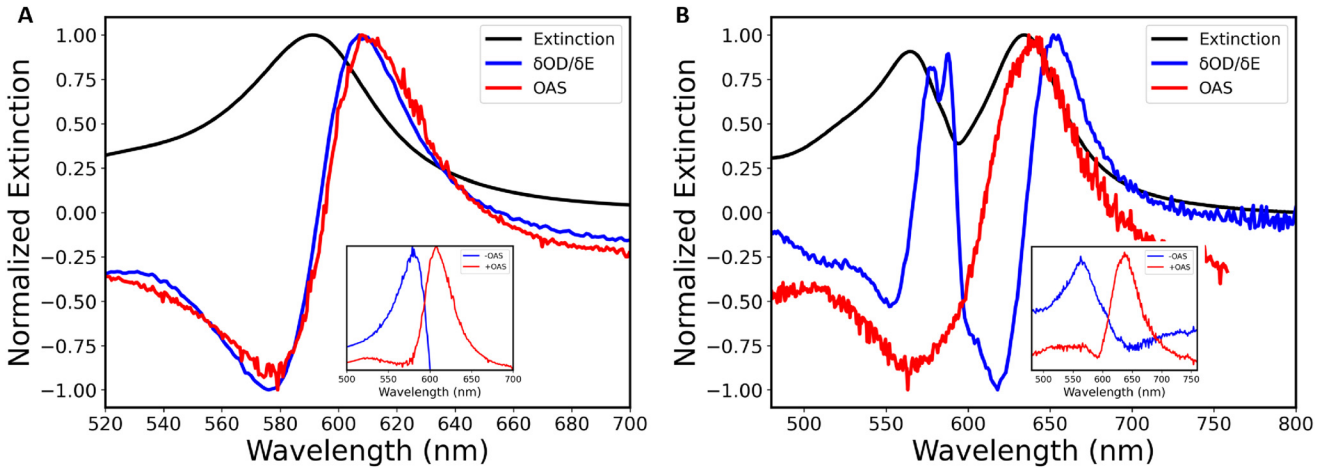

Fig. 5 Static extinction spectrum and first derivative of static extinction for LSPR = 595 nm bare nanoparticles (A) and polariton hybrid (B). Inset: static extinction spectrum with OAS added or subtracted.

Here $\omega_p(t) = \omega_p(0) + \Delta\omega\sin(\omega_a t + \delta)$ and $\Delta\omega$ indicates the magnitude of the variation in plasmon frequency arising from acoustic mode excitation, ω_a is the frequency of the exciton mode, and δ is a phase that varies with timing of the ultrafast pulse. Here we note that $\Delta\omega$ depends on factors such as the pulsed laser intensity and frequency, with the two polaritons showing out-of-phase oscillations because of the ±. Also, this formula assumes that there is only one plasmon and one acoustic mode; more general expressions would involve a sum over many modes.

To describe the extinction spectrum, we assume a Lorentzian lineshape for the extinction (or absorption) $A(\omega)$ of the polaritons as a function of frequency ω:

$$A(\omega, t) = a_{\pm}(t)\frac{\frac{\eta_{\pm}(t)}{\pi}}{(\omega - \omega_{\mathrm{pol}\pm}(t))^2 + {\eta_{\pm}}^2(t)}. \quad (3)$$

Here $a_{\pm}(t)$ is an amplitude for excitation of each polariton and $\eta_{\pm}(t)$ is the linewidth. This formula includes for the possibility oscillations in the lineshape parameters due to the acoustic oscillations of $\omega_p(t)$. This would make sense, since the oscillating plasmons could easily influence the intensity and width in the lineshape.

To describe the transient absorption spectrum, we take the difference between absorptions for the second and first pulse. This yields the expression:

$$\Delta A(\omega(t); t) = \Delta a_{\pm}(t)\frac{\frac{\eta_{\pm}(t)}{\pi}}{(\omega - \omega_{\mathrm{pol}\pm}(t))^2 + {\eta_{\pm}}^2(t)} \quad (4)$$

where the absorption ΔA has both an oscillating variation on time due to the acoustic mode oscillations, as well as a slower time dependence that arises from excited state dynamics as bleaching relaxes. The fast and slow time evolution also applies to $\omega_{\mathrm{pol}\pm}(t)$ and $\eta_{\pm}(t)$. One of the predictions of eqn (4) is that when ΔA is evaluated at multiples of the oscillation frequency, as in Fig. 2C, the only variation in lineshape is due to the slow time variation of the amplitude $\Delta a_{\pm}(t)$ and width $\eta_{\pm}(t)$. The values of $\Delta a_{\pm}(t)$ are negative for the two polaritons, but a similar expression can be developed for the excited state absorption region, where the amplitude parameter $\Delta a(t)$ would be positive.

Conclusions

We have shown that gold tetrahedral nanoparticles can couple strongly to J-aggregate-forming TDBC dye molecules and achieve a Rabi splitting energy of ~206 meV. This large coupling strength is likely a result of the sharp corners and edges of the tetrahedra, enhancing EM field confinement. In comparison with other previously studied polaritonic nanoparticle-dye systems, nanotetrahedra can be additionally synthetically tuned *via* corner sharpness; the degree to which this influences coupling could be a topic of future work. We further demonstrated that, depending on the phase of the phonon and initial LSPR resonance position, the plasmon resonance can shift into more or less resonant conditions with the J-aggregate exciton peak that results in shifts of the extinction coefficient derived from the hybrid polariton states.

Methods

Gold nanotetrahedra capped in CTAC were synthesized according to the literature, the details of which are provided in the SI, and dispersed in water. For each sample, a 200 μL colloidal dispersion with an optical density of 0.4 in a 1 mm cuvette was prepared, to ensure that each sample had approximately the same number of nanoparticles. Although the nanoparticle size will impact O.D., all samples are in a very small size range and thus this is a reasonable approximation. To each sample, 12 μL of a 1 mM TDBC solution was added, and the sample

was left overnight to allow time for assembly of the dye on the nanotetrahedra. Samples were centrifuged at 3500 rpm for 5 min, and precipitated pellets were redispersed in water. A distinct color change was observed upon assembly.

Transient absorption measurements were performed using an amplified Ti:sapphire laser (800 nm, 80 fs pulse duration, 5 kHz rep rate). Of this output, 90% was sent to an optical parametric amplifier to produce the 450 nm pump pulse and the remaining 10% was mechanically time-delayed and focused into a sapphire crystal to generate the white light continuum probe pulse. The pump pulse was mechanically chopped to 2.5 kHz to probe the sample before and after photoexcitation.

Conflicts of interest

There are no conflicts to declare.

Data availability

The MATLAB code for transient absorption and oscillation associated spectral analysis can be found at: https://github.com/kirschner21/OscillationAssociatedSpectra.

Supplementary information (SI): gold tetrahedral nanoparticle synthesis and TEM images of all samples at 3 different magnifications. See DOI: https://doi.org/10.1039/d5nr03987h.

Acknowledgements

B. M. C., L. X. C., and R. D. S. acknowledge the support from the Ultrafast Initiative of the U.S. Department of Energy, Office of Science, Office of Basic Energy Sciences, through Argonne National Laboratory under Contract No. DE-AC02-06CH11357. F. C., Y. W., and X. Y. were supported by the U.S. National Science Foundation under award CHE-2239441. G. C. S. acknowledges the support from the National Science Foundation award 2347622. Work performed at the Center for Nanoscale Materials, a U.S. Department of Energy Office of Science User Facility, was supported by the U. S. DOE, Office of Basic Energy Sciences, under Contract No. DE-AC02-06CH11357.

References

1 R. F. Ribeiro, L. A. Martínez-Martínez, M. Du, J. Campos-Gonzalez-Angulo and J. Yuen-Zhou, Polariton chemistry: controlling molecular dynamics with optical cavities, *Chem. Sci.*, 2018, **9**(30), 6325–6339, DOI: 10.1039/C8SC01043A.

2 E. Cao, W. Lin, M. Sun, W. Liang and Y. Song, Exciton-plasmon coupling interactions: from principle to applications, *Nanophotonics*, 2018, **7**(1), 145–167, DOI: 10.1515/nanoph-2017-0059.

3 D. E. Gómez, S. S. Lo, T. J. Davis and G. V. Hartland, Picosecond Kinetics of Strongly Coupled Excitons and Surface Plasmon Polaritons, *J. Phys. Chem. B*, 2013, **117**(16), 4340–4346, DOI: 10.1021/jp306830s.

4 M. Hertzog, M. Wang, J. Mony and K. Börjesson, Strong light–matter interactions: a new direction within chemistry, *Chem. Soc. Rev.*, 2019, **48**(3), 937–961, DOI: 10.1039/C8CS00193F.

5 A. P. Manuel, A. Kirkey, N. Mahdi and K. Shankar, Plexcitonics – fundamental principles and optoelectronic applications, *J. Mater. Chem. C*, 2019, **7**(7), 1821–1853, DOI: 10.1039/C8TC05054F.

6 M. Pelton, Modified spontaneous emission in nanophotonic structures, *Nat. Photonics*, 2015, **9**(7), 427–435, DOI: 10.1038/nphoton.2015.103.

7 K. J. Russell, T.-L. Liu, S. Cui and E. L. Hu, Large spontaneous emission enhancement in plasmonic nanocavities, *Nat. Photonics*, 2012, **6**(7), 459–462, DOI: 10.1038/nphoton.2012.112.

8 G. M. Akselrod, C. Argyropoulos, T. B. Hoang, C. Ciracì, C. Fang, J. Huang, D. R. Smith and M. H. Mikkelsen, Probing the mechanisms of large Purcell enhancement in plasmonic nanoantennas, *Nat. Photonics*, 2014, **8**(11), 835–840, DOI: 10.1038/nphoton.2014.228.

9 Q. Zhao, W. Zhou, Y. Deng, Y. Zheng, Z. Shi, L. Ang, Z. Zhou and L. Wu, Plexcitonic strong coupling: unique features, applications, and challenges, *J. Phys. D: Appl. Phys.*, 2022, **55**, 203002, DOI: 10.1088/1361-6463/ac3fdf.

10 P. Vasa, W. Wang, R. Pomraenke, M. Lammers, M. Maiuri, C. Manzoni, G. Cerullo and C. Lienau, Real-time observation of ultrafast Rabi oscillations between excitons and plasmons in metal nanostructures with J-aggregates, *Nat. Photonics*, 2013, **7**(2), 128–132, DOI: 10.1038/nphoton.2012.340.

11 F. M. Balci, S. Sarisozen, N. Polat and S. Balci, Colloidal Nanodisk Shaped Plexcitonic Nanoparticles with Large Rabi Splitting Energies, *J. Phys. Chem. C*, 2019, **123**(43), 26571–26576, DOI: 10.1021/acs.jpcc.9b08834.

12 G. P. Wiederrecht, G. A. Wurtz and J. Hranisavljevic, Coherent Coupling of Molecular Excitons to Electronic Polarizations of Noble Metal Nanoparticles, *Nano Lett.*, 2004, **4**(11), 2121–2125, DOI: 10.1021/nl0488228.

13 N. Kometani, M. Tsubonishi, T. Fujita, K. Asami and Y. Yonezawa, Preparation and Optical Absorption Spectra of Dye-Coated Au, Ag, and Au/Ag Colloidal Nanoparticles in Aqueous Solutions and in Alternate Assemblies, *Langmuir*, 2001, **17**(3), 578–580, DOI: 10.1021/la0013190.

14 R. Thomas, A. Thomas, S. Pullanchery, L. Joseph, S. M. Somasundaran, R. S. Swathi, S. K. Gray and K. G. Thomas, Plexcitons: The Role of Oscillator Strengths and Spectral Widths in Determining Strong Coupling, *ACS Nano*, 2018, **12**(1), 402–415, DOI: 10.1021/acsnano.7b06589.

15 F. Würthner, T. E. Kaiser and C. R. Saha-Möller, J-Aggregates: From Serendipitous Discovery to Supramolecular Engineering of Functional Dye Materials,

Angew. Chem., Int. Ed., 2011, **50**(15), 3376–3410, DOI: 10.1002/anie.201002307.

16 N. Peruffo, F. Mancin and E. Collini, Plexcitonic Nanohybrids Based on Gold Nanourchins: The Role of the Capping Layer, *J. Phys. Chem. C*, 2021, **125**(36), 19897–19905, DOI: 10.1021/acs.jpcc.1c05862.

17 N. T. Fofang, T.-H. Park, O. Neumann, N. A. Mirin, P. Nordlander and N. J. Halas, Plexcitonic Nanoparticles: Plasmon–Exciton Coupling in Nanoshell–J-Aggregate Complexes, *Nano Lett.*, 2008, **8**(10), 3481–3487, DOI: 10.1021/nl8024278.

18 A. Yoshida, N. Uchida and N. Kometani, Synthesis and Spectroscopic Studies of Composite Gold Nanorods with a Double-Shell Structure Composed of Spacer and Cyanine Dye J-Aggregate Layers, *Langmuir*, 2009, **25**(19), 11802–11807, DOI: 10.1021/la901431r.

19 M. Tavis and F. W. Cummings, Exact Solution for an N-Molecule–Radiation-Field Hamiltonian, *Phys. Rev.*, 1968, **170**(2), 379–384, DOI: 10.1103/PhysRev.170.379.

20 S. Balci, B. Kucukoz, O. Balci, A. Karatay, C. Kocabas and G. Yaglioglu, Tunable Plexcitonic Nanoparticles: A Model System for Studying Plasmon–Exciton Interaction from the Weak to the Ultrastrong Coupling Regime, *ACS Photonics*, 2016, **3**(11), 2010–2016, DOI: 10.1021/acsphotonics.6b00498.

21 N. T. Fofang, N. K. Grady, Z. Fan, A. O. Govorov and N. J. Halas, Plexciton Dynamics: Exciton–Plasmon Coupling in a J-Aggregate–Au Nanoshell Complex Provides a Mechanism for Nonlinearity, *Nano Lett.*, 2011, **11**(4), 1556–1560, DOI: 10.1021/nl104352j.

22 N. Peruffo, F. Mancin and E. Collini, Ultrafast Dynamics of Multiple Plexcitons in Colloidal Nanomaterials: The Mediating Action of Plasmon Resonances and Dark States, *J. Phys. Chem. Lett.*, 2022, **13**(28), 6412–6419, DOI: 10.1021/acs.jpclett.2c01750.

23 P. Vasa, R. Pomraenke, G. Cirmi, E. De Re, W. Wang, S. Schwieger, D. Leipold, E. Runge, G. Cerullo and C. Lienau, Ultrafast Manipulation of Strong Coupling in Metal–Molecular Aggregate Hybrid Nanostructures, *ACS Nano*, 2010, **4**(12), 7559–7565, DOI: 10.1021/nn101973p.

24 D. Finkelstein-Shapiro, P.-A. Mante, S. Sarisozen, L. Wittenbecher, I. Minda, S. Balci, T. Pullerits and D. Zigmantas, Understanding radiative transitions and relaxation pathways in plexcitons, *Chem*, 2021, **7**(4), 1092–1107, DOI: 10.1016/j.chempr.2021.02.028.

25 T. Simon, D. Melnikau, A. Sánchez-Iglesias, M. Grzelczak, L. M. Liz-Marzán, Y. Rakovich, J. Feldmann and A. S. Urban, Exploring the Optical Nonlinearities of Plasmon-Exciton Hybrid Resonances in Coupled Colloidal Nanostructures, *J. Phys. Chem. C*, 2016, **120**(22), 12226–12233, DOI: 10.1021/acs.jpcc.6b04658.

26 G. V. Hartland, Coherent Excitation of Vibrational Modes in Metallic Nanoparticles, *Annu. Rev. Phys. Chem.*, 2006, **57**(1), 403–430, DOI: 10.1146/annurev.physchem.57.032905.104533.

27 M. S. Kirschner, W. Ding, Y. Li, C. T. Chapman, A. Lei, X.-M. Lin, L. X. Chen, G. C. Schatz and R. D. Schaller, Phonon-Driven Oscillatory Plasmonic Excitonic Nanomaterials, *Nano Lett.*, 2018, **18**(1), 442–448, DOI: 10.1021/acs.nanolett.7b04354.

28 M. S. Kirschner, Y. Jeong, A. P. Spencer, N. E. Watkins, X.-M. Lin, G. C. Schatz, L. X. Chen and R. D. Schaller, Phonon-induced plasmon-exciton coupling changes probed via oscillation-associated spectra, *Appl. Phys. Lett.*, 2019, **115**(11), 111903, DOI: 10.1063/1.5116836, (accessed 7/29/2025).

29 Y. Zheng, W. Liu, T. Lv, M. Luo, H. Hu, P. Lu, S.-I. Choi, C. Zhang, J. Tao, Y. Zhu, *et al.*, Seed-Mediated Synthesis of Gold Tetrahedra in High Purity and with Tunable, Well-Controlled Sizes, *Chem. – Asian J.*, 2014, **9**(9), 2635–2640, DOI: 10.1002/asia.201402499.

30 Y. Wang, J. Chen, Y. Zhong, S. Jeong, R. Li and X. Ye, Structural Diversity in Dimension-Controlled Assemblies of Tetrahedral Gold Nanocrystals, *J. Am. Chem. Soc.*, 2022, **144**(30), 13538–13546, DOI: 10.1021/jacs.2c03196.

31 B. M. Chandler, D. Dey, Y. Wang, X. Ye, G. C. Schatz, L. X. Chen and R. D. Schaller, Coherent Phonon Dynamics in Plasmonic Gold Tetrahedral Nanoparticle Ensembles, *J. Phys. Chem. Lett.*, 2024, **15**(38), 9686–9691, DOI: 10.1021/acs.jpclett.4c02146.

32 M. Kumar, J. Dey, S. Swaminathan and M. Chandra, Shape Dependency of the Plasmon–Exciton Interaction at the Nanoscale: Interplay between the Plasmon Local Density of States and the Plasmon Decay Rate, *J. Phys. Chem. C*, 2022, **126**(18), 7941–7948, DOI: 10.1021/acs.jpcc.2c00701.